

# Effect of the chemical nature of different transition metal ferrocyanides to entrap Cs

Agnès Grandjean<sup>1,2</sup> · Carole Delchet<sup>1,3</sup> · Jérémy Causse<sup>1</sup> · Yves Barré<sup>2</sup> · Yannick Guari<sup>3</sup> · Joulia Larionova<sup>3</sup>

Received: 31 January 2015 / Published online: 27 March 2015  
© Akadémiai Kiadó, Budapest, Hungary 2015

**Abstract** Transition metal ferrocyanides are used since many years to selectively entrap radio-caesium from nuclear contaminated effluents. We investigate the cesium sorption properties on a series of ferrocyanides containing different transition metal ions ( $\text{Ni}^{2+}$ ,  $\text{Co}^{2+}$  and  $\text{Cu}^{2+}$ ) and outline the role of the chemical nature of the bivalent metal ion, the iron oxidation state, the presence of  $\text{K}^+$  in the structure and the grain size of the powders on the equilibrium time and efficiency of the  $\text{Cs}^+$  sorption.

**Keywords** Decontamination · Cs removal · Solid phase separation · Ferrocyanides

## Introduction

Nuclear installations, reactors, or reprocessing plants, but also research facilities, and laboratories generate a large amount of radioactive liquid wastes. Treating this wastewater is required to remove contaminants before it is discharged to the environment to reduce risks posed to human and environmental health.

While the chemical composition of industrial effluents is very heterogeneous, decontamination processes developed at industrial scale are relatively limited. Currently, the most widely used processes consist of evaporation or chemical treatment [1, 2]. Evaporation allows high decontamination factors but cannot be applied to effluents with a high salt content. In this case a co-precipitation method based on in situ precipitation of solid particles to selectively extract one or more radioelements can be used [3]. Alternatively, adsorption methods consisting on the employment of solid sorbents to selectively entrap the radionuclide can also be applied to this kind of effluent.

Radiocesium is one of the most abundant radioactive contaminant and most radiotoxic for the environment and human health. It is found as a nuclear fission product produced routinely in specific confined environment in nuclear plants or accidentally released as in the case of the Fukushima Daiichi accident [4]. There are various methods for removing radiocesium from liquid waste using co-precipitation or adsorption processes. For example, tetraphenylborate developed in the 80s at Savannah River to remove radiocesium from effluent [5], silicotitanate [6], natural or synthetic zeolite [7] or inorganic phosphate [8, 9] have been proposed in literature to selectively adsorb cesium. Nevertheless the most efficient sorbents for removal  $\text{Cs}^+$  from contaminated aqueous effluents over a wide pH and salinity range are the bulk coordination polymers based on transition metal ferrocyanides [10–12]. For instance at *la Hague* facilities, bulk Ni–K ferrocyanide composition in the form of micrometric particles is actually used to selectively precipitate  $\text{Cs}^+$  from contaminated effluent.

Prussian blue is the oldest transition metal ferrocyanide synthesized as a colorant in 1706 in Germany. Its IUPAC name is iron (III) hexacyanoferrate (II) with chemical formula  $\text{Fe}_3[\text{Fe}(\text{CN})_6]_4 \cdot 14\text{H}_2\text{O}$ , that crystallizes in a cubic

✉ Agnès Grandjean  
agnes.grandjean@cea.fr

<sup>1</sup> Institut de Chimie Séparative de Marcoule, ICSM, UMR 5257 CEA-CNRS-UM2-ENSCM, BP 17171, 30207 Bagnols sur Cèze, France

<sup>2</sup> CEA, DEN, DTCD, Laboratoire des Procédés Supercritiques et de Décontamination, BP 17171, 30207 Bagnols sur Cèze, France

<sup>3</sup> Institut Charles Gerhardt Montpellier, ICGM, UMR 5253 CNRS-UM2-ENSCM-UM1, Ingénierie Moléculaire & Nano-Objets, Place E. Bataillon, 34095 Montpellier Cedex 5, France

lattice. Ferrocyanides are a series of related compounds obtained by substitution of the iron in the coordination unit with other transition metal ions or by inclusion of different monovalent cations that balance the negative charge of the coordination unit giving therefore the general formula  $\text{Cat}_x\text{M}_y[\text{Fe}(\text{CN})_6]_z \cdot n \text{H}_2\text{O}$  (where “Cat” means alkali metal or ammonium cation, M is a bivalent transition metal ions such as  $\text{Cu}^{2+}$ ,  $\text{Zn}^{2+}$ ,  $\text{Co}^{2+}$ ,  $\text{Ni}^{2+}$  or  $\text{Fe}^{2+}$ ). Different crystalline structures are available depending on the iron oxidation state and also on the presence or not of the monovalent cation inside the tetrahedral sites of the network.

Cesium sorption properties by using few selected ferrocyanides have been investigated during few recent decades, but it is quite difficult to compare their sorption efficiency since sorption experiments have been performed in different conditions. Furthermore, the lack of detailed samples characterizations precludes the understanding of the proposed sorption mechanisms. For instance, the structure and the sorption properties of the copper hexacyanoferrate with different iron oxidation state (II or III) without counter cation and the potassium–copper hexacyanoferrate (II) have been studied in the 1990 s [10–12]. More recently, adsorption kinetic and equilibrium experiments on copper hexacyanoferrate ( $\text{Fe}^{\text{II}}$ ) have been conducted leading to the determination of some model parameters like pseudo-second order or Langmuir models [13]. A comparative study between copper hexacyanoferrates with different iron oxidation state has shown that the  $\text{Cu}^{\text{II}}\text{Fe}^{\text{III}}$  analogous adsorbs only a small amount of cesium in a surface process whereas  $\text{Cu}^{\text{II}}\text{Fe}^{\text{II}}$  presents a high exchange capacity. This latter is able to adsorb ion pairs ( $\text{Cs}^+/\text{NO}_3^-$ ) thanks to a structural transformation into new phases including large quantities of cesium. On the other hand, mixed potassium–copper hexacyanoferrate (II) ( $\text{K}_2\text{Cu}[\text{Fe}^{\text{II}}(\text{CN})_6]$ ) shows exchange properties between the potassium inserted into the tetrahedral sites of the crystalline structure and the cesium from the liquid phase. But in this case, the “inter-cage” space of the  $\text{K}_2\text{Cu}[\text{Fe}(\text{CN})_6]$  triclinic structure leads to slow sorption kinetics and prevents total exchange even after several months of contact if the solid powder presents a micron size grain [7–9].

In the case of the mixed potassium–nickel hexacyanoferrate(II) of formula  $\text{K}_{0.87}\text{Ni}_{1.57}[\text{Fe}^{\text{II}}(\text{CN})_6]$ , the  $\text{Cs}^+$  sorption mechanism has been studied by varying the particle size of samples [10, 12]. The kinetics data suggest that the  $\text{Cs}^+$  sorption is governed by diffusion through the tunnels of the FCC structure. In this case, the maximum amount of  $\text{Cs}^+$  sorbed by the solid is close to the initial content of  $\text{K}^+$ , suggesting a simple monovalent cationic exchange as sorption mechanism. However, it is not possible to compare these studies with the previously described involved copper hexacyanoferrates (II) due to the

different experimental conditions. Another study on the mixed potassium–nickel hexacyanoferrate(II) concludes that the low K/Fe ratio leads to an increase of the  $\text{Cs}^+$  sorption capacity and an increase of the uptake rate [14]. On the other hand, Ismail team has observed on this type of compounds a modification of the crystalline structure with the incorporation of  $\text{Cs}^+$  [15] and demonstrated high capacity of sorption [16]. Nevertheless, neither the analyzed composition, nor the chemical nature of the samples is given. It is therefore difficult to link the structural, morphological and chemical characteristics of these samples with the  $\text{Cs}^+$  sorption. Note also that to the best of our knowledge, pure cobalt hexacyanoferrate (III) and nickel hexacyanoferrate (III) without monovalent cations have never been studied for their  $\text{Cs}^+$  sorption. Furthermore, since a few years, numerous hybrid composite materials made of organic or inorganic supports loaded with hexacyanoferrate-based particles have been proposed for cesium removal [17–29]. The nature of the metal-hexacyanoferrate particles differs from a research group to another and also from the way of synthesis used for the elaboration of these composites.

Consequently, despite numerous reports on employment of ferrocyanides to selective sorption of  $\text{Cs}^+$ , there is a lack of comparative study on the sorption properties of different ferrocyanides in the same experimental conditions. The present article proposes to compare the sorption kinetic and the sorption isotherm for a series of transition metal ferrocyanides and investigates the effects of the structural, morphological and chemical nature on the sorption properties. Three metal-hexacyanoferrates (III) containing different bivalent transition metal ion ( $\text{Ni}^{2+}$ ,  $\text{Co}^{2+}$  or  $\text{Cu}^{2+}$ ) and a potassium–mixed nickel hexacyanoferrate (III) are then compared. Their sorption properties are discussed with regards to their composition, structure and iron oxidation state, as well as to the grain size of powders.

## Experimental

### Materials and samples preparation

*The different operations and reactions are performed in ambient conditions*

The cobalt hexacyanoferrate (III) (named CoFC) compound was prepared by using previously described procedures from  $\text{Co}(\text{BF}_4)_2$  and  $(\text{TetraButylAmmonium})_3[\text{Fe}(\text{CN})_6]$  precursors [30]. The nickel hexacyanoferrate (III) (named NiFC), and copper hexacyanoferrate (III) (named CuFC) compounds were synthesised using the similar procedure from respectively  $\text{Ni}(\text{BF}_4)_2$  or  $\text{Cu}(\text{BF}_4)_2$  and  $\text{TBA}_3[\text{Fe}(\text{CN})_6]$ . The elemental analyses, performed by the

“Service Central d’Analyse” (CNRS, Vernaison, France) for the obtained powders (see Table 1) permit to obtain the following M to Fe ratio : Co/Fe = 1.59; Ni/Fe = 1.6 and Cu/Fe = 1.7 : Some potassium from the precursors used for the synthesis of  $\text{TBA}_3[\text{Fe}(\text{CN})_6]$  is sometimes found in the solid in trace amounts.

The synthesis of the potassium nickel hexacyanoferrate (III) compound (named KNiFC) was performed thanks to the usual industrial process by mixing a solution containing  $9 \text{ g L}^{-1}$  of  $\text{K}_4\text{Fe}(\text{CN})_6$  and a solution containing  $7 \text{ g L}^{-1}$  of  $\text{NiSO}_4$ , so that the Ni to Fe ratio was equal to 1.2. The elemental analysis of the obtained powder gives the non-stoichiometric composition with Ni to Fe ratio equal to 1.3 and K to Fe iron equal to 1.1. [14].

### Characterizations

Diffraction data were collected using a Bragg–Brentano diffractometer in the  $\theta/\theta$  geometry, with a Cu anticathode ( $\lambda(\text{K}\alpha_1) = 1.54060 \text{ \AA}$ ,  $\lambda(\text{K}\alpha_2) = 1.54439 \text{ \AA}$ , 40 kV, 20 mA) and the high resolution LynxEye detector from Brücker D8 Advance diffractometer. The angular range  $2\theta = 10\text{--}70^\circ$  was scanned at  $0.08^\circ \text{ min}^{-1}$  using  $0.02008^\circ$  steps. The diffractograms were corrected for background and the full-width at half maximum intensity (FWHM) was measured for the main three peaks. The crystallite size  $D$  of the each phase can be obtained from the measured FWHM using Scherrer equation:

$$D = \frac{k\lambda}{\beta \cos \theta}, \quad (1)$$

where  $k$  is a correction factor taken as 0.89,  $\lambda$  is the wavelength of the Cu  $\text{K}\alpha$  line ( $\lambda = 1.54060 \text{ \AA}$ ),  $\theta$  is the Bragg angle of the selected line and  $\beta = (B^2 - b^2)^{1/2}$  with  $B$  the FWHM and  $b$  the resolution parameter of the diffractometer. This last parameter  $b$  was measured on silicon, and is equal to  $0.0865^\circ$  at  $2\theta = 28.4^\circ$ .

Infra-red spectra were performed with the FT-IR Spectrum 100 from PerkinElmer. Spectra are recorded in the range  $400\text{--}4000 \text{ cm}^{-1}$  with a scanning resolution of  $4 \text{ cm}^{-1}$ , in ATR mode. The IR spectra were corrected for the background line using the Spectrum PerkinElmer software.

Scanning Electron Microscopy measurements were performed with a Philips Quanta 200 operating at 15 kV equipped with a Bruker detector. System software for EDX analysis was developed by Bruker.

$\text{Cs}^+$  and  $\text{K}^+$  concentration in aqueous solution used for sorption experiment were analysed using ionic chromatography (from Dionex). Solutions were injected in a column as mobile phase at  $30^\circ\text{C}$ . Cs and K species are retained on the stationary phase and are then eluted after 45 min and analyzed by conductivity. Co, Ni, Cu and Fe content in the remaining solution was also checked using inductively coupled plasma atomic emission spectroscopy (Thermo Scientific).

### Sorption experiments

$\text{Cs}^+$  sorption experiments on each powder sample were performed in batch mode under shaking at room temperature.

The sorption kinetics tests were conducted in batch mode by contacting 20 mg of solid into 20 mL of a solution containing initially  $2 \text{ mmol L}^{-1}$  of nitrate cesium for CuFC, CoFC and NiFC, and initially  $5 \text{ mmol L}^{-1}$  of nitrate cesium for KNiFC. Each point from the kinetics curve corresponds to a single sorption test. After contact, the solution containing the solid is then filtered with a  $2 \mu\text{m}$  membrane and Cs is analyzed by ionic chromatography whereas Cu, Co, or Ni are analyzed using ICP-AES.

The experimental conditions used for the sorption isotherms are 10 mg of solid (NiFC, CuFC, CoFC or KNiFC) shaking into 20 mL of pure water containing different

**Table 1** Main physicochemical characteristics of the studied compound before and after  $\text{Cs}^+$  sorption

Sample	M/Fe ratio*	Powder pattern reference**	IR $\nu(\text{CN}) \text{ Fe}^{\text{II}} \text{ cm}^{-1}$	IR $\nu(\text{CN}) \text{ Fe}^{\text{III}} \text{ cm}^{-1}$	Crystallite size (nm)
CuFC	1.7	$\text{Cu}_3[\text{Fe}^{\text{III}}(\text{CN})_6]_2$	2097	2173	21
CuFC + $\text{Cs}^+$		$\text{K}_2\text{Cu}[\text{Fe}^{\text{II}}(\text{CN})_6]$	2100	2173	32
CoFC	1.59	$\text{Co}_3[\text{Fe}^{\text{III}}(\text{CN})_6]_2$	2095	2157	20
CoFC + $\text{Cs}^+$		Unchanged	2104	2159	24
NiFC	1.6	$\text{Ni}_3^{\text{II}}[\text{Fe}^{\text{III}}(\text{CN})_6]_2$	–	2164	9
NiFC + $\text{Cs}^+$		Unchanged	2100	2165	13
KNiFC	1.3	$\text{K}_2\text{Ni}[\text{Fe}^{\text{II}}(\text{CN})_6]$	2083	–	10
KNiFC + $\text{Cs}^+$		$+\text{Cs}_2\text{Ni}[\text{Fe}^{\text{II}}(\text{CN})_6]$	2087	–	10

\* Elemental analysis

\*\* PXRD measurements

amount of Cs salt (nitrate) from 0.1 to 5 mmol L<sup>-1</sup>, during 24 h.

The sorption experiments in trace concentration and with competing cation were conducted by using enriched sea water solution containing Na<sup>+</sup> (9.6 g L), Ca<sup>2+</sup> (0.4 g L), Mg<sup>2+</sup> (1.28 g L<sup>-1</sup>), K<sup>+</sup> (0.5 g L<sup>-1</sup>) and Sr<sup>2+</sup> (7.8 mg L<sup>-1</sup>), as well as radioactive <sup>137</sup>Cs<sup>+</sup> (8.9 ng L, 28.5 kBq L). 10 mg of solid were added to 20 mL of radioactive solution and mixed during 24 h. The solid was filtered off and the remaining Cs<sup>+</sup> in solutions was analyzed by scintillation.

## Results and discussion

### Characterization of the powders

#### Structural characterization

Figure 1a–d shows XRD pattern of the four studied samples before and after cesium sorption.

All the peaks for KNiFC diffractogram can be indexed with the reference K<sub>2</sub>NiFe<sup>II</sup>(CN)<sub>6</sub> (JCP2.2CA file number 00-020-0915) except the peak at 30.5°, which could be attributed to the presence of a small amount of KNiFe<sup>III</sup>(CN)<sub>6</sub> in agreement with the chemical composition. The crystallinity of KNiFC samples depends on the potassium stoichiometry in the structure: for K/Fe ratio of 1.15 (close to 1.1 of our sample), the product presents higher crystallinity and larger crystallite size compared to other K/Fe ratio [14].

This XRD pattern shows a small structural modification after Cs<sup>+</sup> sorption according to the experimental diffractogram (see Fig. 1a): all peaks are slightly shifted to lower angles, and the peak at 54.5° disappears, that can be explained by formation of Cs<sub>2</sub>NiFe<sup>II</sup>(CN)<sub>6</sub> (JCP2.2CA file number 00-024-0285). This fact indicates that the sorption of Cs<sup>+</sup> is linked with the monovalent cation exchange, as already observed in literature [15].

All the peaks for the NiFC and CoFC diffractograms (respectively Fig. 1b, c) can be indexed with the references Ni<sub>3</sub>[Fe<sup>III</sup>(CN)<sub>6</sub>]<sub>2</sub> (file JCP2.2CA: 01-082-2283) and Co<sub>3</sub>[Fe<sup>III</sup>(CN)<sub>6</sub>]<sub>2</sub> (file JCP2.2CA: 01-082-2284), which show the formation a face-centered cubic structure of F-43 m type. No any modification of the diffractograms were observed after sorption experiments, meaning that Cs<sup>+</sup> insertion within the CoFC or NiFC structures implies no structural modification. However, a different situation is observed with copper-based ferrocyanides. Indeed, all the peaks of the CuFC diffractogram can be indexed with the reference Cu<sub>3</sub>[Fe<sup>III</sup>(CN)<sub>6</sub>]<sub>2</sub> (file JCP2.2CA: 01-070-2702). But in this case, the sorption of Cs<sup>+</sup> within this compound leads to a slight modification of the structure: a decrease of the relative intensity of the peaks at 15.2°, 40° and 54°.

These differences can be explained by the insertion of Cs<sup>+</sup> inside the tetrahedral sites of the network. Unfortunately the reference pattern of the structural phase Cs<sub>2</sub>Cu[Fe<sup>II</sup>(CN)<sub>6</sub>] is not available, but this phase can be indexed by the structural K<sub>2</sub>Cu[Fe<sup>II</sup>(CN)<sub>6</sub>] phase, that must be similar than Cs<sub>2</sub>Cu[Fe<sup>II</sup>(CN)<sub>6</sub>].

The crystallite size *D*(*nm*) of each phase were obtained from the measured FWHM using Scherrer equation (see Eq. (1)) as reported in Table 1. KNiFC and NiFC exhibit crystallite sizes around 10 nm, whereas CuFC and CoFC show crystallite sizes of around 20 nm. The same range of crystallite sizes were observed in the cases of Cu<sup>II</sup>Fe<sup>III</sup> and Cu<sup>II</sup>Fe<sup>II</sup> obtained by a precipitation process [4]. Insertion of Cs<sup>+</sup> inside the structure of KNiFC does not modify the crystallite size, whereas a small increase of these latter is observed for other metal hexacyanoferrates: from 9 to 13 nm for NiFC, from 21 to 32 nm for CuFC and from 20 to 24 nm for CoFC.

#### Infra-red spectroscopy

Infra-red spectroscopy is a sensitive probe of cyanide group and can give interesting information about the iron oxidation state and coordination of the cyanide ligand. In each IR spectrum, the peak around 3400 cm<sup>-1</sup> is assigned to the presence of the interstitial water and OH<sup>-</sup> groups in the network and the peak near 1610 cm<sup>-1</sup> is due to the deformation vibration of the free water molecules [31].

The IR spectra of KNiFC, NiFC, CoFC and CuFC before and after Cs<sup>+</sup> sorption are shown in Fig. 2a–d and the characteristic peaks in the cyanide stretching region are reported in Table 1.

The sharp and strong absorption peaks in the spectral window 2000–2200 cm<sup>-1</sup> are related to the cyanide stretching vibrations and depends on the kind of the metal hexacyanoferrate studied. Indeed relative to ferrocyanide (Fe<sup>II</sup>), the ν(CN) vibration of ferricyanide (Fe<sup>III</sup>) is observed at higher frequency (at around 80 cm<sup>-1</sup> higher) that is explained by the higher ability of ferric ions to receive electron density from the CN<sup>-</sup> ligand [32]. On the other hand, the bivalent transition metal ion also influences the cyanide stretching vibration because it is linked to the electronegativity of the transition metal of the compound in the order ν(CN) Cu<sup>2+</sup> > ν(CN) Ni<sup>2+</sup> > ν(CN) Co<sup>2+</sup> [32, 33].

Infra-red spectra of KNiFC are similar before and after Cs<sup>+</sup> sorption with the cyanide stretching vibration observed respectively at 2083 and 2087 cm<sup>-1</sup>, attributed to the bridging cyano group Fe<sup>II</sup>–CN–Ni<sup>II</sup>.

The Infra-red spectrum of Nickel hexacyanoferrate (III) (NiFC) before cesium sorption shows a unique peak centered at 2164 cm<sup>-1</sup> in the cyanide stretching vibration region characteristic of the bridging cyano ligand Fe<sup>III</sup>–CN–

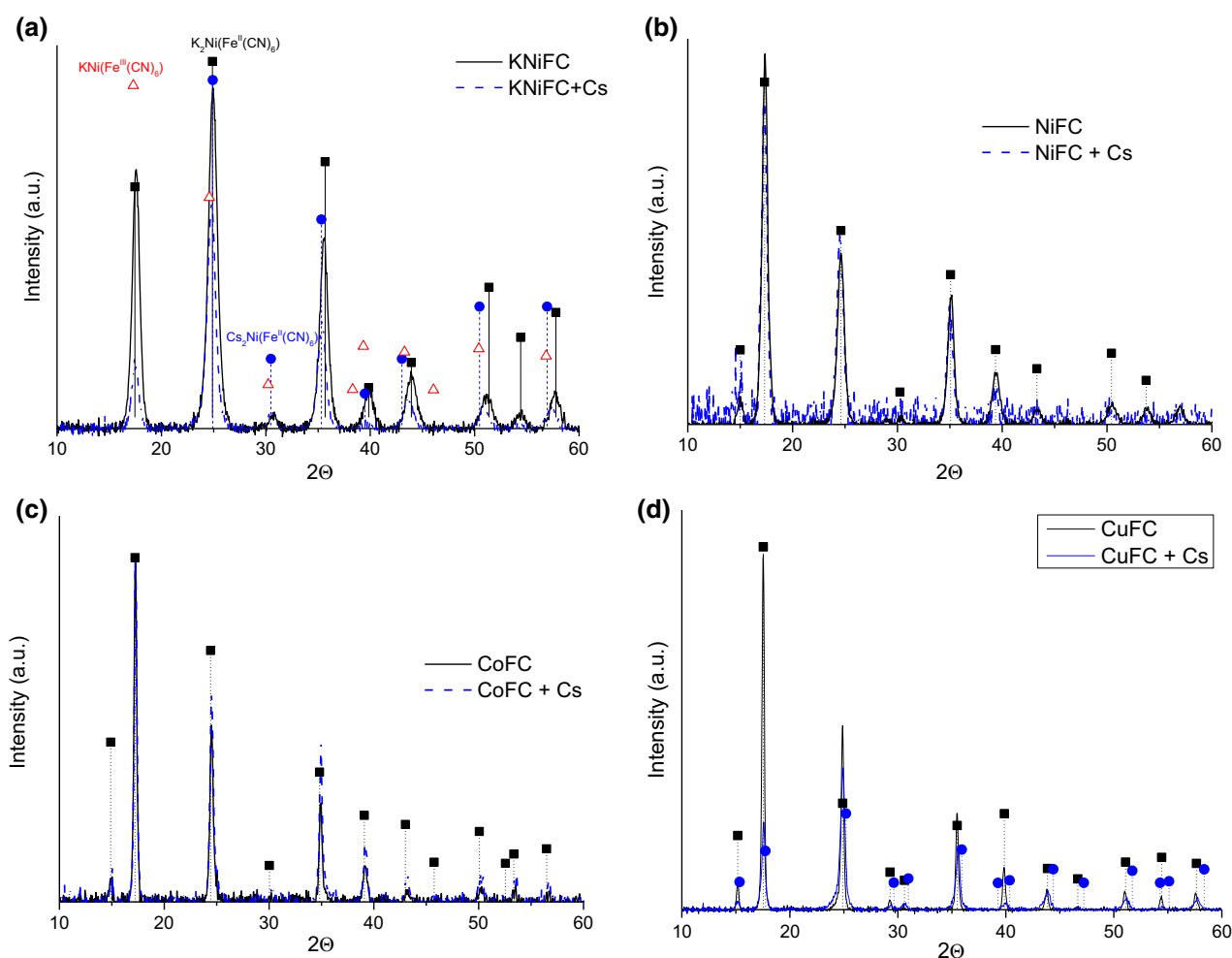


**Fig. 1** **a** XRD powder pattern for the KNiFC (solid line) and for the same sample KNiFC after Cs sorption (dash line) compared with the XRD powder pattern references (filled black square)  $K_2NiFe^{II}(CN)_6$  (file JCP2.2CA: 00-020-0915); (filled blue circle)  $KNiFe^{III}(CN)_6$  (file JCP2.2CA: 00-089-8978); and (open red triangle)  $Cs_2NiFe^{II}(CN)_6$  (file JCP2.2CA: 00-024-0285). **b** XRD powder pattern for the NiFC (solid line) and for the same sample NiFC after Cs sorption (dash line) compared with the XRD powder pattern references (filled black square)  $Ni_3[Fe^{III}(CN)_6]_2$  (file JCP2.2CA: 01-082-2283). **c** XRD

powder pattern for the CoFC (solid line) and for the same sample CoFC after Cs sorption (dash line) compared with the XRD powder pattern references (filled black square)  $Co_3[Fe^{III}(CN)_6]_2$  (file JCP2.2CA: 01-082-2284). **d** XRD powder pattern for the CuFC (solid line) and for the same sample CuFC after Cs sorption (dash line) compared with the XRD powder pattern references (filled black square)  $Cu_3[Fe^{III}(CN)_6]_2$  (file JCP2.2CA: 01-070-2702); (filled blue circle)  $K_2CuFe^{II}(CN)_6$  (file JCP2.2CA: 01-075-0023). (Color figure online)

$Ni^{II}$  [32]. This result is consistent with the chemical analysis and the XRD diffraction pattern.

The Infra-red spectra of both CuFC and CoFC samples show two peaks. The first peak at 2173 and 2157  $cm^{-1}$  for CuFC and CoFC respectively, corresponds to the bridging cyanide stretching vibration for  $Fe^{III}-CN-M^{II}$  coordination while the second one, observed at 2097 and 2095  $cm^{-1}$  for CuFC and CoFC respectively, is usually attributed to the presence of  $Fe^{II}-CN-M^{II}$  bridge. This fact suggests a partial reduction of iron during the synthesis, as usually reported [32, 34].

For the three samples studied, the sorption of  $Cs^+$  leads to a large modification of the IR spectra with an appearance of a peak at 2100  $cm^{-1}$  for NiFC or with an increase of the

relative peak intensity of high frequency bands (2095 and 2097  $cm^{-1}$ ) for CoFC and CuFC related to the  $Fe^{II}-CN-M^{II}$  coordination mode. This fact suggests further reduction of the Fe(III) to Fe(II) in samples during the sorption process.

#### SEM observations

Due to the precipitation methods used for the synthesis of the different powders, the grain size for the product differs. The morphology of the powdered samples were observed by SEM. For KNiFC, NiFC and CoFC, the grain size of the powder varies from 1  $\mu m$  to 100  $\mu m$ . In contrast, the sample CuFC exhibits a colloidal behavior: after the

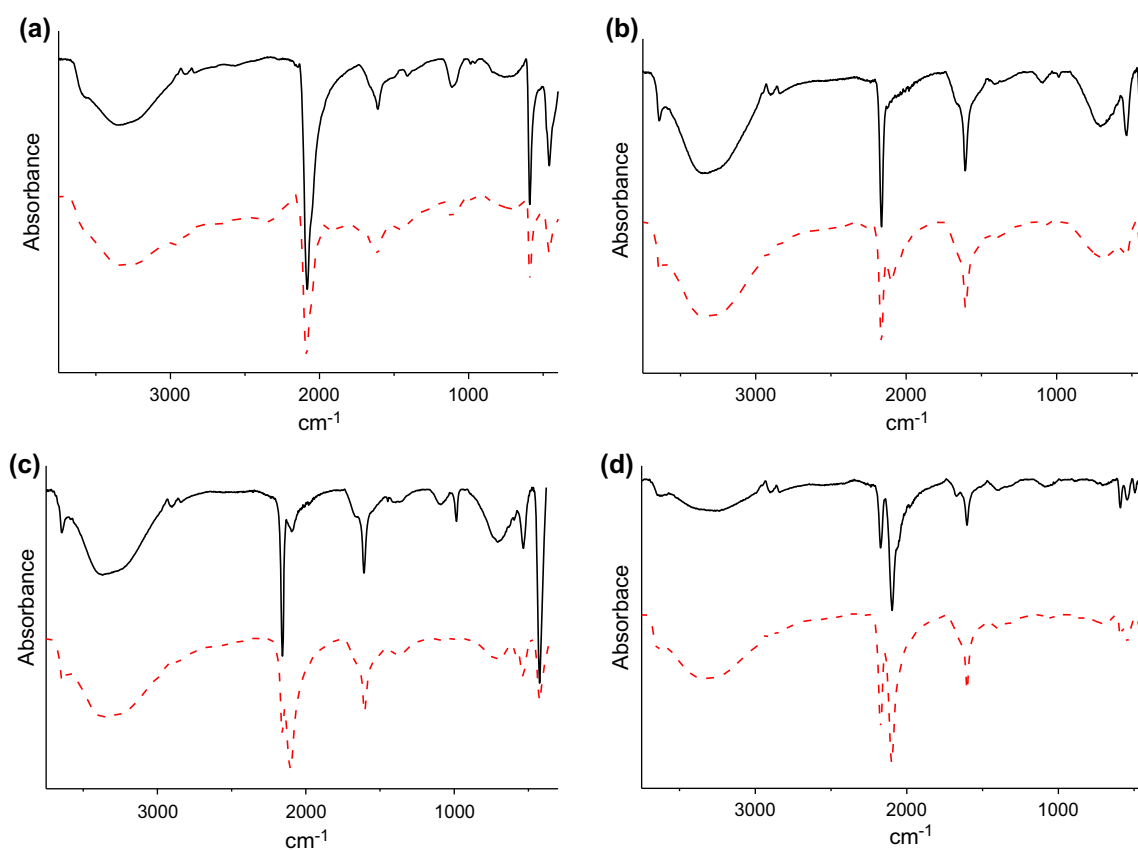


**Fig. 2** Infra-red Spectra (*solid line*) before Cs sorption and (*dash line*) after Cs sorption for **a** KNiFC, **b** NiFC, **c** CoFC and **d** CuFC

synthesis, a stable colloidal suspension of CuFC is obtained, with grain size around 100 nm. It has already been reported that in case of KNiFC the grain size varies with the ratio K/Fe, with the largest grain size for K/Ni between 1.15 and 1.32 [14].

## Sorption study

### Kinetics experiments

The sorption kinetics tests were conducted in a batch mode by contacting 20 mg of solid into 20 mL of a solution containing initially 2 mmol L<sup>-1</sup> of cesium nitrate for CuFC, CoFC and NiFC, and initially 5 mmol L<sup>-1</sup> of cesium nitrate for KNiFC. Each point from the kinetic curves shown on Fig. 3 corresponds to a unique sorption test. Experiments were performed from 10 min to 4 days. After the specific time period, the powder was separated from the solution by filtration through a 0.2 μm cellulose acetate membrane and the remaining Cs<sup>+</sup> concentration of the supernatant was analyzed using ionic chromatography whereas Cu, Co, or Ni are analyzed using ICP-AES. The adsorbed cesium quantity ( $Q_t$  in mmol L<sup>-1</sup>) at time  $t$  is expressed as followed:

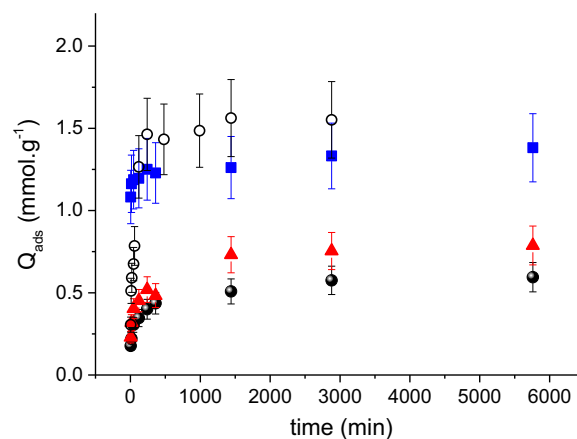


**Fig. 3** Kinetics of Cs sorption for each compound studied (*filled black circle*) NiFC, (*filled red triangle*) CoFC, (*filled blue square*) CuFC, and (*open white circle*) KNiFC. (Color figure online)

$$Q_t = (C_0 - C_t) \frac{V}{m}, \quad (2)$$

where  $C_0$  (mmol L<sup>-1</sup>) is the initial concentration of cesium,  $C_t$  (mmol L<sup>-1</sup>) is the remaining concentration of cesium in solution after the specified time  $t$  (min),  $V$  (L) is the volume of the solution and  $m$  (g) is the mass of solid used.



These kinetic experiments show that for NiFC and CoFC the time to reach equilibrium is close to 1 day (about 1500 min). This result is in agreement with literature where it is reported that sorption of Cs by alkali free hexacyanoferrate ( $\text{Fe}^{\text{III}}$ ) is very slow [10]. For CuFC and KNiFC, the sorption kinetics are faster and equilibrium is reached after about ten minutes.

Secondly, these data allow concluding that there is in the same time sorption of  $\text{Cs}^+$  and desorption of the transition metal initially present in the solid in the case of CoFC, NiFC, and CuFC and desorption of  $\text{K}^+$  in the case of KNiFC. In literature [35–37], whatever the chemical nature of the bivalent transition metal studied, its release is observed with the sorption of  $\text{Cs}^+$  by the solid. Indeed when alkali ions are present inside the hexacyanoferrate structure, it was shown that the Cs sorption occurs thanks to an ionic exchange between this alkali ion from the solid and Cs from the solution [37].

These kinetics data were then fitted using the pseudo-second order kinetics model [38] in order to evaluate the sorption mechanism. The reaction rate of a chemical reaction may be expressed as a function of the reactants concentration. Usually it may be determined by the linearization of the reaction rate. When this reaction involves a solid, the reaction order is also called a pseudo reaction order because it is based on the sorption capacity of the solid. In the most cases involving sorption on a solid, there is a reaction of pseudo second order. The linearization of the reaction rate is describes as follows:

$$\frac{t}{Q_t} = \frac{1}{k_0 Q_e^2} + \frac{t}{Q_e}, \quad (3)$$

where  $k_0$  ( $\text{g mmol}^{-1} \text{min}^{-1}$ ) is the rate constant of pseudo second order adsorption;  $t$  ( $\text{min}$ ) is the time;  $Q_t$  and  $Q_e$  ( $\text{mmol g}^{-1}$ ) are the adsorption capacity at the time  $t$  and at the equilibrium, respectively. If the plot of ( $t/Q_t$ ) as a function of time gives a linear relationship, there is a reaction order and so this sorption is a chemisorption mechanism. This model allows also the determination of the initial rate of sorption given by the term  $k_0 Q_e^2$ .

The analysis of the experimental data for each compound studied with this kinetic model suggests the presence of pseudo second order kinetics, with adjusted  $R$ -square higher than 0.99 in each cases. The parameter of this model for each sample is given in Table 2, as the correlation coefficients  $r^2$ .

These kinetics data and curves fitting show that the adsorption capacity at equilibrium differs with the nature of the hexacyanoferrate used in the order  $Q_e(\text{KNiFC}) > Q_e(\text{CuFC}) > Q_e(\text{CoFC}) > Q_e(\text{NiFC})$ . Moreover the initial rate of sorption given by the term  $k_0 Q_e^2$  follows the same behavior with an initial rate of sorption significantly faster for KNiFC, and CuFC compared to CoFC and NiFC. The copper

hexacyanoferrate exhibits a behavior similar to the mixed potassium–nickel hexacyanoferrate, with a similar initial rate of sorption.

According to the literature, without alkali ions in the structure, the comparison of  $\text{Cu}^{\text{II}}\text{Fe}^{\text{II}}$  and  $\text{Cu}^{\text{II}}\text{Fe}^{\text{III}}$  [10, 12] has shown that in the structure of  $\text{Cu}^{\text{II}}\text{Fe}^{\text{II}}$ , copper atoms occupy two types of sites (Cu1 and Cu2) which is not the case of  $\text{Cu}^{\text{II}}\text{Fe}^{\text{III}}$ . The Cu2 atoms are not linked to iron by cyanide bridges and are expected to be more mobile. The absence of Cu2 sites in  $\text{Cu}^{\text{II}}\text{Fe}^{\text{III}}$  compound should prevent the diffusion of ion pairs and then could explain the lower kinetics and lower capacity. From these studies, the Cs sorption mechanism into  $\text{Cu}^{\text{II}}\text{Fe}^{\text{II}}$  includes at least two steps: first a diffusion of ion pairs (Cs and nitrate) into the solid and the formation of a new solid phase followed by a release of copper which compensates the sorption of Cs. In our case, the behavior of CuFC with faster kinetics and higher capacity than other hexacyanoferrate (CoFC and NiFC) without potassium could be explained by the presence of two phases in the structure;  $\text{CuFe}^{\text{III}}$  and also  $\text{CuFe}^{\text{II}}$  as observed on the IR spectra.

When alkali ions are present in the interstitial sites of the hexacyanoferrate structure, as observed for KNiFC and as reported in literature, the kinetic of sorption is faster [35, 37, 39–41]. In this case, the sorption mechanism is an ionic exchange between this alkali ion from the solid and the Cs from the solution.

#### *Isotherm experiments*

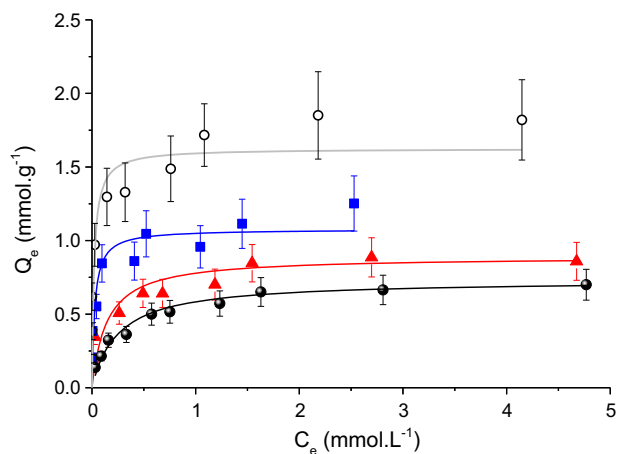
The experimental condition used for the sorption isotherms are 10 mg of solid shaking into 20 mL of pure water containing different amount of nitrate Cs salt from 0.1 to 5  $\text{mmol L}^{-1}$ , during 24 h. This duration time is enough to reach equilibrium. Each solution is then analyzed by ionic chromatography before and after contacting the powder with the solution. The results for each kind of compound are shown on Fig. 4.

Sorption equilibrium is usually described by an isotherm equation such as Langmuir or Freundlich models. The parameters of these models express the surface properties and affinity of the sorbent at a fixed temperature and pH.

The Freundlich empirical model is the earliest sorption isotherm equation [42]. This model was devoted to describe non-ideal sorption on heterogeneous surface or multilayer sorption. This model assumes an exponentially decay of the sorption site distribution when sorption occurs. This Freundlich isotherm model is often criticised because it is empirical and is not founded on a fundamental thermodynamic basis since it does not reduce to Henry's law at low concentration [43]. Then we have applied the Langmuir isotherm model.

**Table 2** Second order model parameters

	CoFC	NiFC	CuFC	KNiFC
$r^2$ Adjusted	0.998	0.998	0.999	0.999
$Q_e$ (mmol g <sup>-1</sup> )	0.8	0.6	1.4	1.6
$k_0 Q_e^2$ (mmol g <sup>-1</sup> min <sup>-1</sup> )	$8 \times 10^{-3}$	$6 \times 10^{-3}$	$4 \times 10^{-2}$	$4 \times 10^{-2}$

**Fig. 4** Sorption isotherm and Langmuir model (filled black circle) NiFC, (filled red triangle) CoFC, (filled blue square) CuFC, and (open white circle) KNiFC. (Color figure online)

The Langmuir isotherm model was developed by Langmuir in 1916 to describe the equilibrium of sorption of gas on a surface as a function of gas pressure [44]. This model is probably the most widely applied sorption isotherm model and described with a good agreement numerous experimental data. This model predicts a monolayer adsorption onto a surface containing a finite number of adsorption sites with no migration of adsorbate on the plane surface [45, 46]. Once a site is filled, no further sorption can take place at that site. This indicates that the surface reaches a saturation point where the maximum adsorption of the surface will be achieved. Moreover, at low sorbate concentrations, this model reduces a linear isotherm and thus follows Henry's law.

This Langmuir isotherm model is described by this equation:

$$Q_e = Q_{\max} \left( \frac{LC_e}{1 + LC_e} \right), \quad (4)$$

where  $Q_e$  (mmol g<sup>-1</sup>) is the equilibrium adsorption capacity of Cs onto the solid;  $Q_{\max}$  (mmol g<sup>-1</sup>) is the maximum sorption capacity;  $C_e$  (mmol L<sup>-1</sup>) is the equilibrium Cs concentration in solution and  $L$  (L mol<sup>-1</sup>) is the Langmuir constant related to the energy of adsorption. Then a “Langmuir” energy of adsorption can simply be defined by this equation:

$$\Delta G_L = -RT \ln(Q_{\max} L). \quad (5)$$

The non-linear form of the Langmuir isotherm equation and the least squares method were applied to determine the isotherm parameters and especially the monolayer adsorption capacity. The results of fitting the experimental data points for all samples studied are shown on Fig. 4 and reported on Table 3. The high correlation coefficient ( $r^2 > 0.99$ ) confirms that Langmuir adsorption isotherm was an appropriate model for the Cs ions adsorption onto ferrocyanides.

These fits are also useful for determining the numerical value of the constant  $Q_{\max}$  which defines the maximum capacity of the studied solids. This allows an accurate comparison between each sample. The maximum sorption capacity obtained through the Langmuir isotherm varies with the chemical nature of the transition metal of each alkali free hexacyanoferrate and with the presence of K inside the structure in the order  $Q_{\max}(\text{KNiFC}) > Q_{\max}(\text{CuFC}) > Q_{\max}(\text{CoFC}) > Q_{\max}(\text{NiFC})$ . This follows the same behavior than the initial rate of sorption obtained thanks to kinetics experiments. The higher maximum sorption capacity of CuFC compared to other compounds without K within the structure (CoFC and NiFC) could be linked even to the grain size of the sample but also to its chemical composition. Indeed, as observed by SEM experiments, NiFC and CoFC powders are in the micron-size range, whereas the CuFC powder is in the nano-size range. This difference implies a larger amount of surface available for Cs adsorption in case of CuFC leading to a higher capacity of the Cu-hexacyanoferrate compared to the other alkali free hexacyanoferrate due to this nano-size effect [17, 29]. But also, it was observed that CuFC shows two phases CuFe<sup>III</sup> and CuFe<sup>II</sup>. Both observations could explain the higher maximum sorption capacity of CuFC compared to CoFC and NiFC.

The KNiFC maximum capacity obtained here is lower than the reported data from literature, where a maximum amount of Cs was estimated to be 2.6 mmol g<sup>-1</sup> [10]. But in this paper, the product used has a K/Ni ratio lower than

**Table 3** Parameters of the Langmuir Isotherm model

	CoFC	NiFC	CuFC	KNiFC
$Q_{\max}$ (mmol g <sup>-1</sup> )	0.9	0.7	1.2	1.6
$L$ (L mol <sup>-1</sup> )	7	4	12	49
$\Delta G$ (kJ mol <sup>-1</sup> )	-4	-3	-6	-11



ours with a composition of  $K_{0.87}Ni_{1.57}Fe^{II}(CN)_6$ . Now, it was proved that lower K/Fe ratio increases the Cs sorption capacity as the sorption rate [14]. This enhancement has been explained by a slight increase in the size of cage windows of mixed potassium–nickel hexacyanoferrate and then a better matching with the Cs<sup>+</sup> size.

The affinity of the solid to Cs<sup>+</sup> ions, given by the parameter *L* from the Langmuir isotherm model is about the same for each free alkali metal-hexacyanoferrate studied (CuFC, NiFC, and CoFC). The Langmuir energy of adsorption is negative, confirming that the sorption is spontaneous and favorable. But these values are relatively low, much lower compared to the value obtained in the case of mixed potassium–nickel hexacyanoferrate (KNiFC).

#### Selectivity experiments in trace concentration

The effect of trace concentration and competing cations was studied using sea water solution [ $Na^+$  (9.6 g L),  $Ca^{2+}$  (0.4 g L),  $Mg^{2+}$  (1.28 g L),  $K^+$  (0.5 g L), and  $Sr^{2+}$  (7.8 mg L)] enriched in  $^{137}Cs^+$  (28.5 kBq L<sup>-1</sup>) onto two representative samples of this study: a free alkali cobalt-hexacyanoferrate and a mixed potassium–nickel hexacyanoferrate. In case of mixed K–nickel hexacyanoferrate, the distribution coefficient  $K_d$  ( $4 \times 10^6$  mL g<sup>-1</sup>) is higher compared to free K Cobalt hexacyanoferrate ( $K_d = 6 \times 10^5$  mL g<sup>-1</sup>). These results confirm a higher selectivity of mixed potassium metal hexacyanoferrate compared to hexacyanoferrate without K within the structure.

## Conclusions

Transition metal ferrocyanides exhibits a great variety of compositions and structures and several stoichiometries may be obtained with the same nature of bivalent transition metal ions and hexacyanometallates. All these parameters may highly influence the sorption efficiency and selectivity. In the series of cation free  $M^{II}-Fe^{III}$  hexacyanoferrates studied here, the sorption capacity and the sorption rate increase in the range of bivalent metal ion:  $Ni^{2+} < Co^{2+} < Cu^{2+}$ . All these compounds present closed characteristics and show the iron reduction during the Cs<sup>+</sup> sorption. The relatively modest sorption properties (low capacity and slow kinetics) are explained essentially by a surface sorption mechanism limited by the surface of the grain size. In case of  $Co^{2+}$  based ferrocyanides from this study, even if a small peak corresponding to the  $Fe^{II}-CN-Co^{II}$  bridge has been observed on IR spectra, we can consider on the basis of elemental analysis and the XRD diffractogram that the sample corresponds mostly to  $Co_3[Fe^{III}(CN)_6]_2$ . The kinetics of sorption is just a bit faster and the sorption capacity is higher in comparison with the  $Ni^{2+}$  based analogous. For these compounds

$M-Fe^{III}$ , the sorption properties are explained essentially by a surface sorption mechanism limited by the surface of the grain size.

The studied  $Cu^{2+}$ -based ferrocyanides may exhibit two phases: one corresponding to  $Cu_3[Fe^{III}(CN)_6]_2$  and the second one to  $Cu_2[Fe^{II}(CN)_6]$ . The presence of this later containing  $Fe^{II}$  should allow the faster sorption rate and the higher capacity, according to what is reported in literature [10]. Due to the difference in their structures, the  $Fe^{II}$ -based compound is more able to transform its structure for the insertion of a large quantity of Cs<sup>+</sup>.

When alkali ions are already present within the structure, the sorption mechanism is an ionic exchange and the kinetics is fast and the capacity is high [35–37]. This was confirmed with the sample KNiFC of this study which exhibit the faster sorption kinetics and the higher sorption capacity of all samples studied. Nevertheless, the amount of exchangeable potassium in the structure has to be well controlled to improve the rate of sorption and the maximum sorption capacity.

**Acknowledgments** We acknowledge Cyrielle Rey for its help for the analysis of the compounds and of the Cs from solution; Bruno Corso for XRD experiments; Johann Ravaux for SEM experiments; and Véronique Dubois for its help for ICP-AES analysis. This work was supported financially by CEA, University of Montpellier and MEMFIS ANR project.

## References

1. Szoke S, Patzay G, Weiser L (2003) *Radiochim Acta* 91:229–232
2. Rao SVS, Paul B, Lal KB, Narasimhan S, Ahmed J (2000) *J Radioanal Nucl Chem* 246:413–418
3. Flouret J, Barre Y, Muhr H, Plasari E (2012) *Chem Eng Sci* 77:176–183
4. Thakur P, Ballard S, Nelson R (2013) *Sci Total Environ* 458:577–613
5. Peterson RA, Burgess JO, Walker DD, Hobbs DT, Serkiz SM, Barnes MJ, Jurgensen AR (2001) *Sep Sci Technol* 36:1307–1321
6. Hritzko BJ, Walker DD, Wang NHL (2000) *AIChE J* 46:552–564
7. Borai EH, Harjula R, Malinen L, Paajanen A (2009) *J Hazard Mater* 172:416–422
8. Ma B, Oh S, Shin WS, Choi SJ (2011) *Desalination* 276:336–346
9. Reddy VN, Satyanarayana J, Kumar SS, Sivaiah MV, Krishna RM, Lakshminarayana S, Murthy GS (2004) *Indian J Chem Technol* 11:479–485
10. Ayrault S, Jimenez B, Garnier E, Fedoroff M, Jones DJ, Loos-Neskovic C (1998) *J Solid State Chem* 141:475–485
11. Loos-Neskovic C, Ayrault S, Badillo V, Jimenez B, Garnier E, Fedoroff M, Jones DJ, Merinov B (2004) *J Solid State Chem* 177:1817–1828
12. Ayrault S, LoosNeskovic C, Fedoroff M, Garnier E, Jones DJ (1995) *Talanta* 42:1581–1593
13. Han F, Zhang GH, Gu P (2013) *J Radioanal Nucl Chem* 295:369–377
14. Mimura H, Kageyama N, Akiba K, Yoneya M, Miyamoto Y (1998) *Solvent Extr Ion Exch* 16:1013–1031

15. Ismail IM, El-Sourougy MR, Moneim NA, Aly HF (1998) *J Radioanal Nucl Chem* 237:97–102
16. Ismail IM, El-Sourougy MR, Moneim NA, Aly HF (1999) *J Radioanal Nucl Chem* 240:59–67
17. Delchet C, Tokarev A, Dumail X, Toquer G, Barre Y, Guari Y, Guerin C, Larionova J, Grandjean A (2012) *RSC Adv* 2:5707–5716
18. Vincent C, Hertz A, Vincent T, Barré Y, Guibal E (2014) *Chem Eng J* 236:A202–A211
19. Okamura Y, Fujiwara K, Ishihara R, Sugo T, Kojima T, Umeno D, Saito K (2014) *Radiat Phys Chem* 94:119–122
20. Ambashta RD, Wattal PK, Singh S, Bahadur D (2003) *J Magn Magn Mater* 267:335–340
21. Ca DV, Cox JA (2004) *Microchim Acta* 147:31–37
22. Chang C-Y, Chau L-K, Hu W-P, Wang C-Y, Liao J-H (2008) *Microporous Mesoporous Mater* 109:505–512
23. Lin YH, Fryxell GE, Wu H, Engelhard M (2001) *Environ Sci Technol* 35:3962–3966
24. Sangvanich T, Sukwarotwat V, Wiacek RJ, Grudzien RM, Fryxell GE, Addleman RS, Timchalk C, Yantasee W (2010) *J Hazard Mater* 182:225–231
25. Valsala TP, Joseph A, Shah JG, Raj K, Venugopal V (2009) *J Nucl Mater* 384:146–152
26. Causse J, Tokarev A, Ravaux J, Moloney M, Barre Y, Grandjean A (2014) *J Mater Chem A* 2:9461–9464
27. Turgis R, Arrachart G, Delchet C, Rey C, Barre Y, Pellet-Rostaing S, Guari Y, Larionova J, Grandjean A (2013) *Chem Mater* 25:4447–4453
28. Hu B, Fugetsu B, Yu H, Abe Y (2012) *J Hazard Mater* 217–218:85–91
29. Torad NL, Hu M, Imura M, Naito M, Yamauchi Y (2012) *J Mater Chem* 22:18261–18267
30. Folch B, Guari Y, Larionova J, Luna C, Sangregorio C, Innocenti C, Caneschi A, Guerin C (2008) *New J Chem* 32:273–282
31. Du ZH, Jia MC, Wang XW (2013) *J Radioanal Nucl Chem* 298:167–177
32. Balmaseda J, Reguera E, Rodriguez-Hernandez J, Reguera L, Autie M (2006) *Microporous Mesoporous Mater* 96:222–236
33. de Tacconi NR, Rajeshwar K, Lezna RO (2003) *Chem Mater* 15:3046–3062
34. Lejeune J, Brubach J-B, Roy P, Bleuzen A (2014) *CR Chim* 17:534–540
35. Loosneskovic C, Fedoroff M (1989) *Solvent Extr Ion Exch* 7:131–158
36. Loosneskovic C, Fedoroff M, Mechherri MO (1990) *Analyst* 115:981–987
37. Haas PA (1993) *Sep Sci Technol* 28:2479–2506
38. Ho YS (2006) *J Hazard Mater* 136:681–689
39. Mimura H, Lehto J, Harjula R (1997) *J Nucl Sci Technol* 34:607–609
40. Lehto J, Harjula R, Wallace J (1987) *J Radioanal Nucl Chem* 111:297–304
41. Vlasselaer S, Dolieslager W, Dhont M (1976) *J Inorg Nucl Chem* 38:327–330
42. Freundlich HZ (1906) *J Phys Chem* 57:385–470
43. Desta MB (2013) *J Thermodyn* 2013:6
44. Langmuir I (1916) *J Am Chem Soc* 40:1361–1368
45. Ho YS, Porter JF, McKay G (2002) *Water Air Soil Pollut* 141:1–33
46. Hameed BH, Din ATM, Ahmad AL (2007) *J Hazard Mater* 141:819–825